2004-04-30

Controller Switching Policy in Flexible Plates Using PZT Actuators Subject to Spatiotemporal Variations of Disturbances

Taraneh Moghani
Worcester Polytechnic Institute

Controller Switching Policy in Flexible Plates Using PZT Actuators Subject to Spatiotemporal Variations of Disturbances

by

Taraneh Moghani

A Thesis

Submitted to the Faculty

of the

WORCESTER POLYTECHNIC INSTITUTE

in partial fulfillment of the requirements for the

Degree of Master of Science

in

Mechanical Engineering

by

April 2004

APPROVED:

Professor Michael A. Demetriou, Advisor

Professor Gretar Tryggvason, Committee Member

Professor Zhikun Hou, Committee Member

Professor John Sullivan, Graduate Committee Representative

Abstract

The primary goal of this thesis is to evaluate vibration control of an all-clamped plate having an unknown disturbance. The vibration control is implemented using a piezoelectric actuator placed at an optimal location.

The first part of this thesis considers a robust actuator placement with respect to varying spatial distributions of disturbances. The treatment here, is different from performance-based LQR approaches, since it is based on minimizing the effect of the disturbance distributions.

The second part of this thesis addresses a more general case where the plate is under an unknown disturbance. An unknown disturbance is also characterized by the case where the disturbance signal moves randomly over the entire spatial domain. An optimal switching controller algorithm is developed, based on LQR performance, which switches between piezoelectric actuators employed for the vibration control of the plate. A single actuator is selected from the various actuator locations during each time interval, which leads to performance enhancement.

Acknowledgements

I gratefully thank my advisor Prof. Demetriou for his constant guidance and supervision during my studies and research at WPI.

My special thanks to Prof. Tryggvason and Prof. Sullivan for their support and advice during my studies at WPI. I would like to thank my friends Ganapathy Raman and Adriana Hera, for all their technical supports. My thanks to my friend Sia Najafi for all his help and support during my studies.

I would specially thank my best friend, Eric L. Herrman for all his support in tough times and his technical guidance during my research and studies at WPI. Above all, I would like to thank my parents and my brothers Mehdi and Hamid for all their love, encouragements and support during my academic career.

Contents

List of Figures

List of Tables

Chapter 1

Introduction

1.1 Literature Review

Vibration control of plates has always presented a challenge due to the complexity of the vibration modes. Because the plate spans two-dimensions, the concept is much more difficult than evaluating a 1D case such as a beam structure. This requires the controllability and observability enhancement for all combinations of plate modes within 2D span [1].

Plate vibrations were first studied experimentally by Chlandi in 1787. He observed nodal patterns on square plates at their natural frequencies [2]. Since then, due to the wide applications of flexible plates in aerospace engineering, civil engineering, shipbuilding engineering, and other fields, the theory of plate vibrations has developed rapidly. Currently, one of the most important research areas on this topic has been the vibration control of plates by using smart actuators.

The use of smart actuators such as PZT patches to control the vibration of flexible structures is currently a research subject of great interest. This is due to the fact that piezoelectric materials have mechanical simplicity, small volume, are

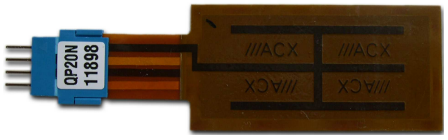

Figure 1.1: A piezoelectric actuator/sensor.

light-weight and can easily be integrated into structures [4]. When a stress field is applied to these materials, an electrical charge is produced on the material surface. This makes it possible to use them as sensors. The converse is also true. When an electric field is applied to a piezoelectric material it changes its shape and size. This gives it the ability to be used as an actuator. A piezoelectric actuator is shown in Figure 1.1. The subject, control of plate vibration and the issue of sensor and actuator placement, has also been addressed in earlier investigations. For example, [5] addresses the optimal placement of collocated piezoelectric actuators and sensors on a simply supported thin plate by using the spatial controllability. In [10], the robust control of a thin all-clamped plate with piezoelectric sensors and actuators is considered, and good locations for the low-frequency modes were evaluated. [15] addresses a placement solution with non-collocated actuators and disturbances, as well as non-collocated performance and sensor output. [16] considers the observability and controllability enhancement in sensing and control effectiveness of the segmented sensors. The problem of optimal actuator placement and switching actuator algorithm are presented for flexible structures in [8] and [9].

1.2 The Objectives of the Current Research

In the present thesis two fundamental cases are addressed and an algorithm for each is developed;

In the first part of this thesis, the case of actuator placement based on robustness with respect to varying distributions of disturbances is considered. [6] suggests that when the spatial distribution of the disturbance is taken into account, the result for the optimal actuator placement is different from the performance-based LQR optimality. This then is verified with numerical results for 1D thermal system. The treatment here is somewhat different in the sense that it is investigated for the two-dimensional case and for the first time for an all-clamped plate. The idea is to control the vibration of the plate in a way such that the effects of the distribution of the disturbances are taken into account. This is for the case that the spatial distribution of disturbances is known. The numerical results of this section were also presented in [20].

The objective of the second part of this thesis is to provide a control algorithm which switches between piezoelectric actuators employed for the vibration control of the flexible plate. The switching actuator implementation is addressed in [8] and [9], and is verified experimentally for a flexible beam in [11]. The supervisory switching actuator considering the spatial disturbance distributions/worst case scenario is presented in [7] for a flexible beam. The present work provides a switching actuator methodology in 2D span, where the plate is having a disturbance in which both temporal and spatial parts are unknown. This can be also implemented for the case that the disturbance signal is moving randomly all over the plate. To control the resulting vibration, multiple piezoelectric actuators are distributed at different locations on the plate. During each time interval, the best actuator which results in

control optimality is activated. The suggested scheme confirms that the switching control algorithm offers a better performance over the single patch (non-switching) control design.

1.3 Chapter Organization

The organization of this thesis is as follows: Chapter 2 briefly describes the mathematical model of the system under study. Chapter 3 discusses controllability enhancement, optimal actuator placement and the observer design. First, the problem formulation for optimal placement of actuators for different non-moving disturbance distributions is considered. In the second phase a switching actuator control policy is applied to a plate having a moving disturbance profile. Finally, the conclusions of the present research and suggestions for future work follow in Chapter 4.

Chapter 2

Mathematical Model

2.1 Plate Model

The general assumptions used in the analysis of the mathematical model of the flexible plate are as follows:

1. The plate is flat and has constant thickness.
2. It is composed of material which is homogenous, linear, elastic and isotropic.
3. The plate is considered in the thin plate category.
4. The thickness of the piezoelectric patches are small enough compared to that of the plate.
5. The plate deforms through flexural deformation. The deformations are small in comparison with the thickness.

The dynamics of a thin uniform plate can be expressed by the differential equation

$$D_E \nabla^4 W(\xi,\zeta,t) + \rho h \ddot{W}(\xi,\zeta,t) + c_d \nabla^4 \dot{W}(\xi,\zeta,t) + \gamma \dot{W}(\xi,\zeta,t) = F(\xi,\zeta,t), \quad (2.1)$$

where D_E is the plate flexural rigidity and is equal to $D_E = Eh^3/(12(1-\nu^2))$, ν is Poisson's ratio, E is Young's Elastic Modulus, ρ is density, and h is the plate thickness. γ and c_d represent *air* damping and *Kevin-Voigt* damping respectively [12]. $W(\xi,\zeta,t)$ is the plate deflection of each point (ξ,ζ) at time t. The operator ∇^4 is given by

$$\nabla^4 W(\xi,\zeta,t) = \frac{\partial^4 W(\xi,\zeta,t)}{\partial \xi^4} + 2\frac{\partial^4 W(\xi,\zeta,t)}{\partial \xi^2 \partial \zeta^2} + \frac{\partial^4 W(\xi,\zeta,t)}{\partial \zeta^4}.$$

The plate vibration is subject to all-clamped boundary condition. This imposes zero displacement and slope at the boundaries expressed by

$$W(0,\zeta,t) = W(a,\zeta,t) = W(\xi,0,t) = W(\xi,b,t) = 0,$$

and

$$\frac{\partial W}{\partial \xi}(0,\zeta,t) = \frac{\partial W}{\partial \xi}(a,\zeta,t) = \frac{\partial W}{\partial \zeta}(\xi,0,t) = \frac{\partial W}{\partial \zeta}(\xi,b,t) = \ 0,$$

where $a \times b \times h$ is the dimension of the plate under study as it is shown in Figure 2.1. The right-hand side term of (2.1), $F(\xi,\zeta,t)$, can include both the disturbance signal term and the forcing function of the actuator device. In the simulation model, a piezoelectric patch is considered to play the role of the actuator. In (2.2), the disturbance and piezoelectric patch terms are shown

$$F(\xi,\zeta,t) = d(\xi,\zeta)w(t) + \frac{\partial^2 M_{p\xi}}{\partial \xi^2} + \frac{\partial^2 M_{p\zeta}}{\partial \zeta^2}, \tag{2.2}$$

where $d(\xi,\zeta)$ is the spatial distribution of the disturbance signal, and $w(t)$ denotes the temporal part of the signal. The controller term is the forcing result of the piezoelectric patch. This term is explained in the next section where the piezoelectric actuator model is provided.

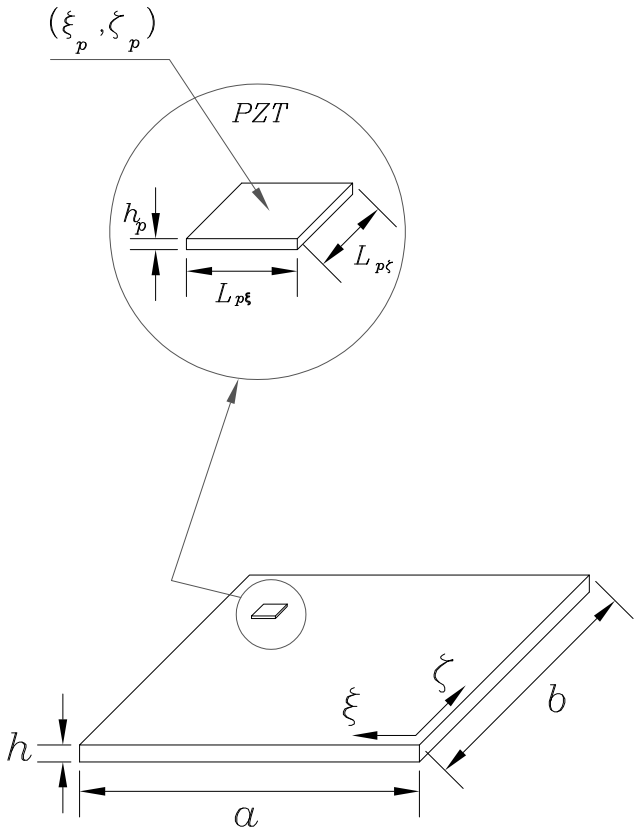

Figure 2.1: A plate with a PZT patch attached.

A mathematical model of the plate using *Galerkin* scheme is provided. In general, closed-form solutions to the partial differential equations describing distributed structures are not possible or feasible. Following the approach given in [12], the solution for the partial differential equation is approximated in the form of

$$W(\xi, \zeta, t) = \sum_{m=1}^{\infty} \sum_{n=1}^{\infty} \phi_{mn}(\xi, \zeta) \eta_{mn}(t), \tag{2.3}$$

where $\phi_{mn}(\xi, \zeta)$ denotes modal function or finite element approximation, and $\eta_{mn}(t)$ represents the generalized function, in which m and n are the indices in (ξ, ζ) space. In practice these functions are dicretized by a finite number of coordinates and this

is generally quite sufficient to account for the low-frequency dynamical behavior in most practical situations [23]

$$W(\xi,\zeta,t) \simeq \sum_{m=1}^{m_\xi}\sum_{n=1}^{n_\zeta} \phi_{mn}(\xi,\zeta)\eta_{mn}(t), \tag{2.4}$$

where m_ξ and n_ζ are the number of modes considered in both ξ and ζ directions. By substituting (2.2) into (2.1), multiplying both sides of (2.1) by a test function ϕ_{kl} and integrating through the entire spatial domain, the plate dynamics is given by

$$M\ddot{\eta} + D_p\dot{\eta} + K\eta = B_1(\xi,\zeta)w(t) + B_2(\xi,\zeta)u(t), \tag{2.5}$$

where η is a vector including the generalized functions

$$\eta = \{\eta_{11}, \eta_{12}, \ldots, \eta_{1n_\zeta}, \ldots, \eta_{m_\xi n_\zeta}\},$$

M, D_p and K are the mass, damping and stiffness matrices of the system respectively, and their related elements are given by

$$\begin{aligned}
M_{kl} &= \rho h \sum_{m=1}^{m_\xi}\sum_{n=1}^{n_\zeta} \int_0^a\int_0^b \phi_{mn}(\xi,\zeta)\phi_{kl}(\xi,\zeta)d\xi d\zeta \\
K_{kl} &= D_E \sum_{m=1}^{m_\xi}\sum_{n=1}^{n_\zeta} \int_0^a\int_0^b \Big(\frac{\partial^4\phi_{mn}(\xi,\zeta)}{\partial\xi^4} + 2\frac{\partial^4\phi_{mn}(\xi,\zeta,t)}{\partial\xi^2\partial\zeta^2} + \frac{\partial^4\phi_{mn}(\xi,\zeta)}{\partial\zeta^4}\Big)\phi_{kl}(\xi,\zeta)d\xi d\zeta \\
D_p &= \alpha_{d1}M + \alpha_{d2}K \\
B_{1kl}(\xi,\zeta) &= \int_0^a\int_0^b d(\xi,\zeta)\phi_{kl}(\xi,\zeta)d\xi d\zeta \\
B_{2kl}(\xi,\zeta)u(t) &= \int_0^a\int_0^b \Big(\frac{\partial^2 M_{p\xi}}{\partial\xi^2} + \frac{\partial^2 M_{p\zeta}}{\partial\zeta^2}\Big)\phi_{kl}(\xi,\zeta)d\xi d\zeta.
\end{aligned} \tag{2.6}$$

Following [14], D_p is known as proportional damping, where the *air* damping and *Kevin-Voigt* damping coefficients are denoted by α_{d1} and α_{d2}, respectively, and are

equal to $\alpha_{d1} = \gamma/\rho h$ and $\alpha_{d2} = c_d/D_E$.

The modal indices of the test function ϕ_{kl} are shown with "k" for ξ and "l" for ζ direction.

Following [13], the function $\phi(\xi, \zeta)$ represents the product of beam functions given by

$$\phi(\xi, \zeta) = \varphi(\xi)\psi(\zeta), \tag{2.7}$$

where $\varphi(\xi)$ and $\psi(\zeta)$ can be chosen as the mode shapes or finite elements satisfying the applied boundary conditions.

2.2 Piezoelectric Model

The ability of piezoelectric material to convert mechanical strains into electrical voltage and vice versa, allows them to be used as actuators and sensors once placed on flexible structures. The use of piezoelectric material as actuator in vibration control is also beneficial because these actuators only excite the elastic modes of the structures without exciting the rigid body modes [5]. This is important since very often only elastic motions of the structures need to be controlled.

The dimension of PZT[1] strip is $L_{p\xi} \times L_{p\zeta} \times h_p$ as it is depicted in Figure 2.1. A piezoelectric moment, M_p, is produced by controlling the applied voltage V_p. Following [23], the moment produced by PZT actuator is given by

$$M_p(t, \xi, \zeta) = \frac{1}{2} E_p d_{31} w_p (h + h_p) \nu_p(\xi, \zeta, t), \tag{2.8}$$

where E_p is the Young's module of the film, d_{ij} is the electric charge constant controlling the extension in the directions normal to that of the electric field, and

[1]Piezoelectric; The abbreviation PZT stands for Plumbum Zirconate Titanate [27].

w_p is the width of the electrodes equal to $L_{p\xi}$ in ζ direction and to $L_{p\zeta}$ in ξ direction. It is assumed that the thickness of the PZT patch is small compared to that of the plate, $h_p \ll h$. ν_p is the applied voltage, whose spatial part is constant in the interval of the piezoelectric length, but following a step function, χ, reaches zero at its boundaries

$$\begin{aligned}\nu_p(t,\xi,\zeta) = V_p(t)\Big[\chi\Big(\xi - (\xi_p - L_{p\xi}/2)\Big) - \chi\Big(\xi - (\xi_p + L_{p\xi}/2)\Big)\Big]\times \\ \Big[\chi\Big(\zeta - (\zeta_p - L_{p\zeta}/2)\Big) - \chi\Big(\zeta - (\zeta_p + L_{p\zeta}/2)\Big)\Big] = V_p(t)\Big(V_{p\xi}(\xi)\times V_{p\zeta}(\zeta)\Big),\end{aligned} \tag{2.9}$$

where (ξ_p,ζ_p) is the center of piezoelectric as shown in Figure 2.1, and $V(t)$ is the applied voltage.

2.3 Finite Element Model

The functions in (2.7) are defined by using the finite elements method based upon the following reasons:

1. The modal shapes of the plate are not available for all-clamped plate having the PZT patches.

2. Using finite element functions instead of eigenfunctions makes it easy to apply changes to boundary conditions without any fundamental changes in the code. By multiplying the representative functions by a transformation matrix, one can set the numerical code for different boundary conditions.

3. The eigenfunctions are global functions, i.e., they extend over the entire domain and tend to be complicated functions, often difficult to work with computationally [12]. By contrast, in the finite element method, the admissible functions are local functions, defined over small sub-domains and equal to zero

identically everywhere else. In addition they tend to be simple functions such as low-degree polynomials [12].

As it is shown in (2.10), cubic splines, [18], are used as the admissible functions

$$\Phi_i(\xi) = \begin{cases} (\xi - \xi_{i-2})^3 & \xi \in [\xi_{i-2}, \xi_{i-1}] \\ \Delta\xi^3 + 3\Delta\xi^2(\xi - \xi_{i-1}) + 3\Delta\xi(\xi - \xi_{i-1})^2 - 3(\xi - \xi_{i-1})^3 & \xi \in [\xi_{i-1}, \xi_i] \\ \Delta\xi^3 + 3\Delta\xi^2(\xi_{i+1} - \xi) + 3\Delta\xi(\xi_{i+1} - \xi)^2 - 3(\xi_{i+1} - \xi)^3 & \xi \in [\xi_i, \xi_{i+1}] \\ (\xi_{i+2} - \xi)^3 & \xi \in [\xi_{i+1}, \xi_{i+2}] \end{cases} . \tag{2.10}$$

To apply the all-clamped boundary condition, $(n+3)$ original spline functions are changed to $(n-1)$ transformed spline functions via the transformation.

$$\{\varphi_1, \varphi_2, \ldots, \varphi_{n-1}\} = \{-2\Phi_{-1} + \Phi_0 - 2\Phi_1, \Phi_2, \ldots, \Phi_{n-2}, -2\Phi_{n-1} + \Phi_n - 2\Phi_{n+1}\}.$$

where Φ_i and φ_i represent the original spline functions and the transformed ones respectively, and following the all-clamped boundary conditions they have the form as follows

$$\begin{cases} \varphi_1 = -2\Phi_{-1} + \Phi_0 - 2\Phi_1 \\ \varphi_2 = \Phi_2 \\ \vdots \\ \varphi_{n-2} = \Phi_{n-2} \\ \varphi_{n-1} = -2\Phi_{n-1} + \Phi_n - 2\Phi_{n+1} \end{cases}$$

The degree of the polynomials is dictated by the differentiability requirement, which is three for the plate problem. φ_i and Φ_i for the case $n = 6$ are shown in Figure 2.2 in ξ direction for $a = 1$. The transformed splines are imposed to be zero at the boundaries which satisfy the all-clamped boundary conditions. The derivative

of the transformed splines are zero at boundaries as shown in Figure 2.3 due to the all-clamped boundary conditions.

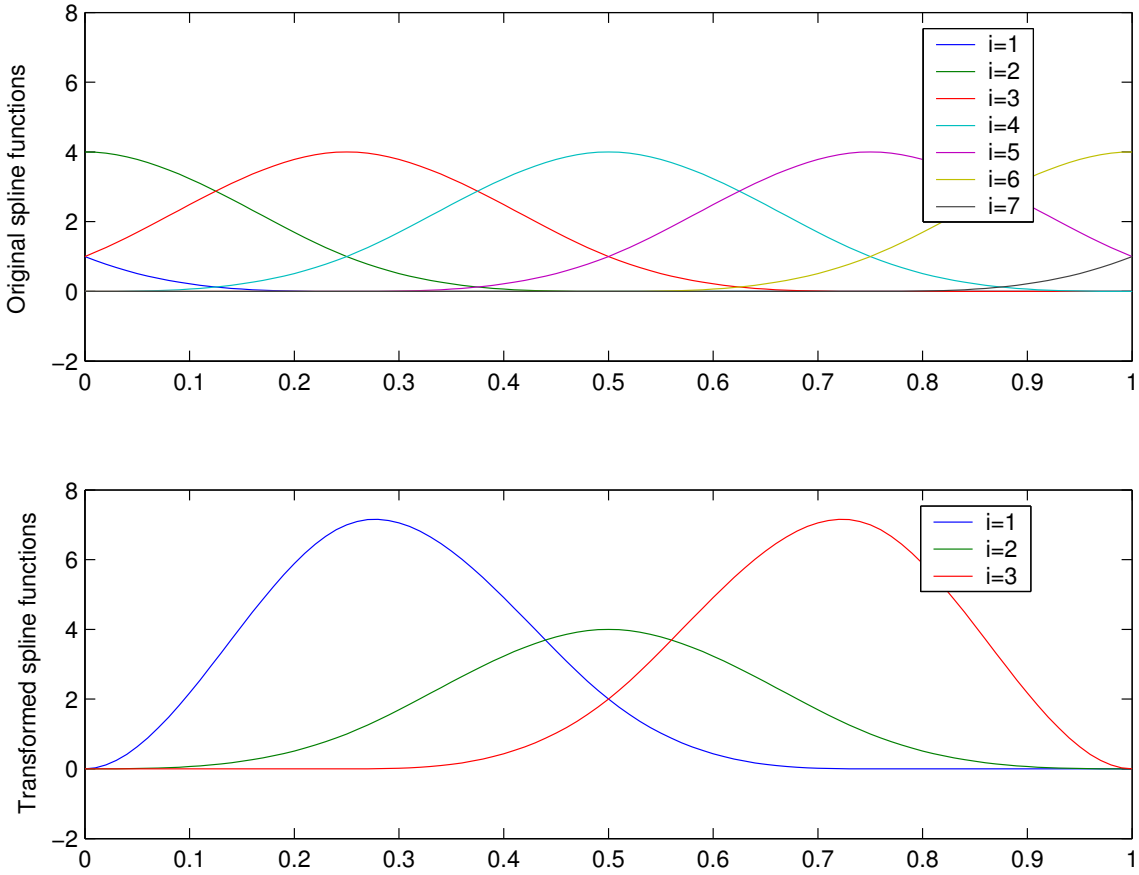

Figure 2.2: Original splines (Φ_i) and transformed splines (φ_i).

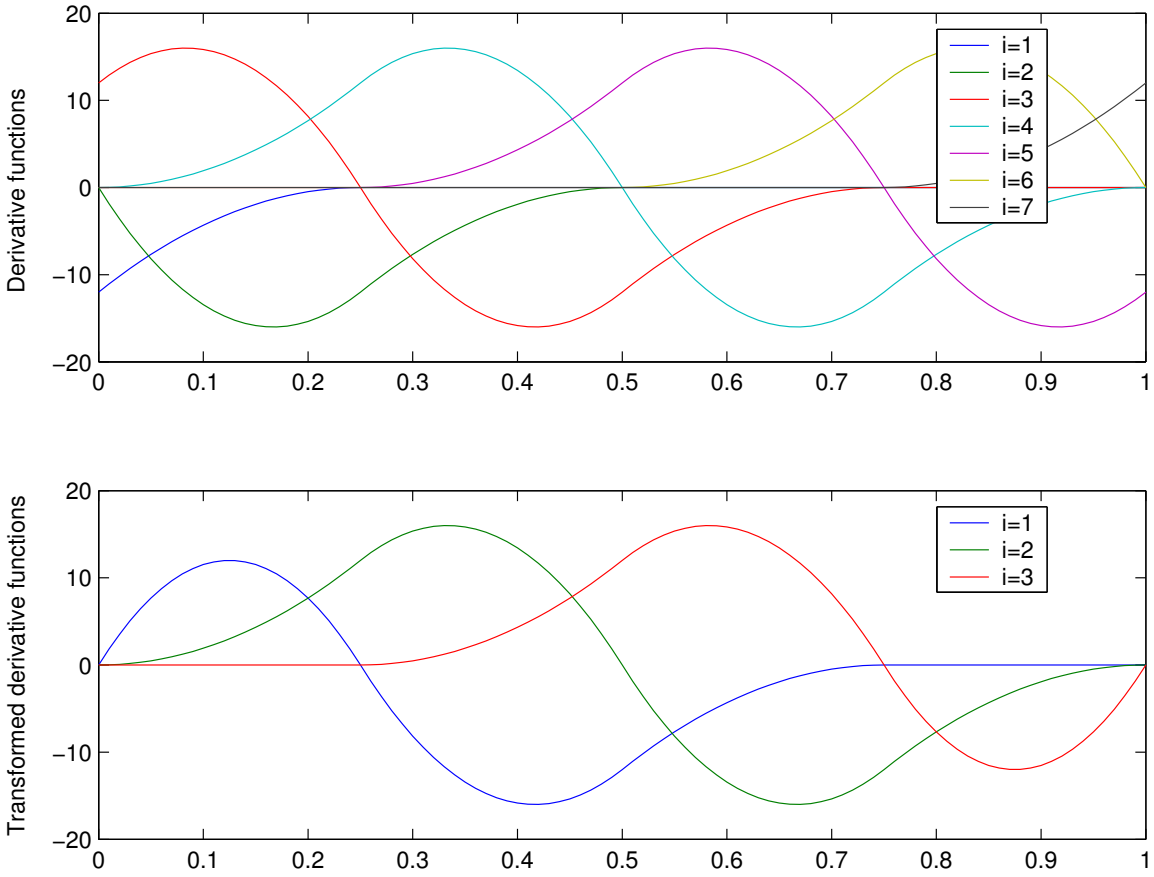

Figure 2.3: Derivative of original splines ($\Phi_i^{'}$) and transformed splines ($\varphi_i^{'}$).

Chapter 3

Optimal Actuator Placement

The idea is to find the best actuator placement to control the vibration of the plate which is under the influence of a disturbance signal. While the goal is to find the best actuator location, one must restrict the search in a subset of controllable locations for the following reasons as it is presented in [20]:" *(i) avoid search over an infinite set of candidate locations with the obvious computational advantages, (ii) avoid regions where the system looses controllability and (iii) incorporate design restrictions and hardware limitations that dictate performance requirements.*" Thus, among a set of controllable actuator candidates the one which results in control optimality, is activated. The issue of sensor and actuator placement has been addressed in earlier investigations such as [15], [16], [17], [11] and [5]. The algorithm here is different, in the sense that in the first part, the optimal actuator placement is based on minimizing the effect of the spatial distributions of disturbances on a certain performance output for an all-clamped plate. In the second part, it is considered that the plate has an unknown disturbance signal which can move randomly all over the spatial domain. Following this, an optimal controller switching policy is provided which switches between the actuators to control the vibration of the plate.

To this end, the state form of the system can be defined by

$$\begin{aligned} \dot{x}(t) &= Ax(t) + B_e w(t) + B_c(\xi, \zeta)u(t) \\ y(t) &= Cx(t), \end{aligned} \tag{3.1}$$

where $w(t)$ is the disturbance temporal part. A, B_e, B_c and C are constant matrices and for the current problem, they have the form

$$\begin{aligned} A &= \begin{bmatrix} 0_{\sigma\times\sigma} & I_{\sigma\times\sigma} \\ -M^{-1}K & -M^{-1}D_p \end{bmatrix}_{2\sigma\times 2\sigma}, \\ B_e &= \begin{bmatrix} 0_{\sigma\times 1} \\ M^{-1}B_1(\xi,\zeta) \end{bmatrix}_{2\sigma\times 1}, B_c = \begin{bmatrix} 0_{\sigma\times 1} \\ M^{-1}B_2(\xi,\zeta) \end{bmatrix}_{2\sigma\times 1}, x = \begin{bmatrix} \eta \\ \dot{\eta} \end{bmatrix}_{2\sigma\times 1}, \end{aligned} \tag{3.2}$$

where $\sigma = m_\xi n_\zeta$, and matrix C is selected with respect to the desired output measurement, where in this part it is assumed to be an identity matrix.

When the external disturbances are insignificant, open-loop control can perform very well. Quite often, however, better results can be obtained with feedback control, in which the control term $u(t)$ takes into consideration the actual response of the system [12]. After applying the state feedback control law $u = -k(\xi_p, \zeta_p)x(t)$, the closed loop form of the system (3.1) becomes

$$\begin{aligned} \dot{x}(t) &= \Big(A - B_c(\xi_p, \zeta_p)k(\xi_p, \zeta_p)\Big)x(t) + B_e w(t) \\ y(t) &= Cx(t). \end{aligned} \tag{3.3}$$

First, one should make sure that the control system is stable. The stability of a linear system is determined by the eigenvalues of the matrix of coefficients. More specifically, the system is merely stable if all the eigenvalues are pure imag-

inary, asymptotically stable if the eigenvalues are real and negative, or complex with negative real part, and unstable if at least one eigenvalue has a positive real part. In the case of open-loop control, stability is governed by the eigenvalues of A. In the case of state feedback control stability is governed by the eigenvalues of $A - B_c(\xi_p, \zeta_p)k(\xi_p, \zeta_p)$.

3.1 Controllable Locations

In this section we explain the concept of state controllability. Controllability addresses the issue of actuation and the ability of the actuators to control the state of the system. For example, if a point force device acts at the nodal point of a vibrating mode of a plate, the system looses controllability for that specific mode. In that case to enhance the controllability, one can search for those locations that are not close to the nodal points of the fundamental modes. In the current model, a piezoelectric patch is used as the actuating controller device. Hence, for controllability purposes following [20] one should search for the locations which ensure the controller term of (2.1) is not near zero as it is given by

$$\frac{\partial^2 M_{p\xi}}{\partial \xi^2} + \frac{\partial^2 M_{p\zeta}}{\partial \zeta^2} \neq 0. \tag{3.4}$$

Finally, the objective is to limit the possible actuator locations

$$\Theta = \Big\{(\xi, \zeta) \in [0, a] \times [0, b]\Big\},$$

to the ones which provide controllability for the fundamental modes.

The dynamical system as (3.1) or the pair (A, B_c) is controllable, if for any initial state and a final desired state, there exists an input $u(t)$ such that leads the solution

of (3.1) to the final desired state. The controllability of a system can be obtained through some algebraic or geometric criteria which are all equivalent and are defined by [21]

1. (A, B_c) is controllable.
2. The matrix $W_c(t) := \int_0^t e^{A\tau} B_c B_c^{'} e^{A^{'}\tau} d\tau$ is positive definite for any $t > 0$.
3. The controllability matrix $[B, AB, A^2B, ..., A^{n-1}B]$ has a full-row rank.
4. The matrix $[A - \lambda I, B_c]$ has full row rank for all λ.
5. If λ and v be any eigenvalue and left eigenvector of A; then $v^{'} B_c \neq 0$.
6. The eigenvalues of $A + B_c K$ can be freely assigned by a suitable choice of K.

By substituting (2.7) into B_2 from (2.6), using partial integration with respect to all-clamped boundary condition, we have

$$\begin{aligned}
&\int_0^a \int_0^b \big(\frac{\partial^2 M_{p\xi}}{\partial \xi^2} + \frac{\partial^2 M_{p\zeta}}{\partial \zeta^2}\big)\varphi_k(\xi)\psi_l(\zeta) d\xi d\zeta = \\
&\int_0^a \int_0^b \frac{1}{2}\frac{\partial^2 \nu_p}{\partial \xi^2} E_p d_{31} w_p h \varphi_k(\xi)\psi_l(\zeta)\, d\xi d\zeta + \int_0^a \int_0^b \frac{1}{2}\frac{\partial^2 \nu_p}{\partial \zeta^2} E_p d_{32} w_p h \varphi_k(\xi)\psi_l(\zeta)\, d\xi d\zeta \\
&= I_1(\xi_p, \zeta_p, k, l) + I_2(\xi_p, \zeta_p, k, l).
\end{aligned} \tag{3.5}$$

Using (2.9), and considering the all-clamped boundary condition

$$\begin{aligned}
I_1(\xi_p, \zeta_p, k, l) &= \frac{1}{2} E_p d_{31} w_p h V_p(t) \int_0^a \frac{d^2 V_{p\xi}}{d\xi^2}\varphi_k(\xi) d\xi \int_0^b V_{p\zeta}\psi_l(\zeta) d\zeta \\
&= \frac{1}{2} E_p d_{31} w_p h V_p(t) \left[\frac{dV_{p\xi}}{d\xi}\varphi_k(\xi)|_0^a - \int_0^a \frac{dV_{p\xi}}{d\xi}\varphi_k^{'}(\xi) d\xi\right] \int_0^b V_{p\zeta}\psi_l(\zeta) d\zeta \\
&= \frac{1}{2} E_p d_{31} w_p h V_p(t) \left[\int_0^a V_{p\xi}\varphi_k^{''}(\xi) d\xi\right] \int_0^b V_{p\zeta}\psi_l(\zeta) d\zeta \\
&= \frac{1}{2} E_p d_{31} w_p h V_p(t) \left[\int_{\xi_p - L_{p\xi}/2}^{\xi_p + L_{p\xi}/2} \varphi_k^{''}(\xi) d\xi\right] \int_{\zeta_p - L_{p\zeta}/2}^{\zeta_p + L_{p\zeta}/2} \psi_l(\zeta) d\zeta.
\end{aligned}$$

Finally, one can write

$$I_1(\xi_p,\zeta_p,k,l)=\frac{1}{2}E_p d_{31} w_p h V_p(t)\Big(\varphi_k^{'}(\xi_p+L_{p\xi}/2)-\varphi_k^{'}(\xi_p-L_{p\xi}/2)\Big)\int_{\zeta_p-L_{p\zeta}/2}^{\zeta_p+L_{p\zeta}/2}\psi_l(\zeta)\,d\zeta$$

$$I_2(\xi_p,\zeta_p,k,l)=\frac{1}{2}E_p d_{32} w_p h V_p(t)\Big(\psi_l^{'}(\zeta_p+L_{p\zeta}/2)-\psi_l^{'}(\zeta_p-L_{p\zeta}/2)\Big)\int_{\xi_p-L_{p\xi}/2}^{\xi_p+L_{p\xi}/2}\varphi_k(\xi)\,d\xi.$$

Thus, one must first find those locations that provide the best controllability; this translates to actuator locations that ensure the controller term satisfies

$$\Big|I_1(\xi_p,\zeta_p,k,l)+I_2(\xi_p,\zeta_p,k,l)\Big|>\varepsilon \tag{3.6}$$

That means the system is controllable for the mode indices (k,l), i.e., the controllability matrix for that mode has a full-rank.

The good locations to control the low-frequency modes are evaluated by using the modal shapes. To find the locations satisfying (3.6), the modal shapes of all-clamped plate are considered as the test functions. These functions are available and given by [13]

$$\begin{aligned}&\phi_{kl}(\xi,\zeta)=\varphi_k(\xi)\psi_l(\zeta)=\\&A_k\Big[\cosh(\epsilon_k\xi/a)-\cos(\epsilon_k\xi/a)-\alpha_k\Big(\sinh(\epsilon_k\xi/a)-\sin(\epsilon_k\xi/a)\Big)\Big]\times\\&A_l\Big[\cosh(\epsilon_l\zeta/b)-\cos(\epsilon_l\zeta/b)-\alpha_l\Big(\sinh(\epsilon_l\zeta/b)-\sin(\epsilon_l\zeta/b)\Big)\Big],\end{aligned} \tag{3.7}$$

where A_k, A_l, ϵ_k and ϵ_l are constant for each mode, and are given for fundamental frequency modes in [13].

By substituting (3.7) into (3.5), the candidate locations which do not satisfy (3.6) are eliminated. Therefore, a final set of N admissible actuator locations of several low but fundamental frequency modes is defined after applying the expressed methodology

Table 3.1: The values of ϵ and α for the first/fundamental modes of an all-clamped plate [13].

l	ϵ_l	α_l
1	4.7300408	0.98250222
2	7.8532043	1.00077731)
3	10.9956078	0.99996645
4	14.1371655	1.00000145
5	17.2787596	0.99999994
6	20.4203522	1.0000000

$$\Theta_p = \Big\{(\xi_p, \zeta_p)\Big|_\ell \in \Theta : (3.6) \text{ is satisfied, } \ell = 1, 2, \ldots, N\Big\}, \tag{3.8}$$

It should be remarked that there is no guarantee for controllability of these selected PZT locations for high frequency modes. However, this methodology provides an enhanced controllability of the closed-loop control system for the fundamental modes. Determination of the control of the entire infinity of modes is not feasible, nor is it necessary. In fact, higher modes have only minimal participation in the motion, as they are difficult to excite. So, the control of a limited number of lower modes is proposed while the number is sufficiently large that the accuracy will not suffer [12].

3.2 Robust Actuator Placement

3.2.1 Robust Control

The objective of a control design is to achieve a desired performance while the stability is maintained. The performance specifications of a control design can be

defined in different ways. One way is to describe the performance specifications of the system in terms of the disturbance signals. For example, for a tracking system this could be defined by the size of the tracking error signal [21], or for the present work this could be presented by measuring the size of the spatial disturbance signal acting on the plate. As it is stated in [21], the $\mathcal{H}^2$ control problem is to find a controller gain that stabilizes the system and minimizes the $\mathcal{H}^2$ norm of the transfer matrix $\|T_{yw}\|_2^2$ from w to y.

Taking into account that A is stable, the $\mathcal{H}^2$ norm of the linear system (3.1) is given by

$$\|T_{yw}\|_2^2 = \text{trace}\Big[B_e^T P_c(\xi_p, \zeta_p) B_e\Big] = \text{trace}\Big[C Q_c(\xi_p, \zeta_p) C^T\Big], \tag{3.9}$$

where $P_c(\xi, \zeta)$ and $Q_c(\xi_p, \zeta_p)$ are the observability and controllability Gramians which are the solutions to following *Lyapunov equations* [21]

$$\begin{aligned} A^T P_c(\xi_p, \zeta_p) + P_c(\xi_p, \zeta_p) A + C^T C = 0, \\ A Q_c(\xi_p, \zeta_p) + Q_c(\xi_p, \zeta_p) A^T + B_e B_e^T = 0. \end{aligned} \tag{3.10}$$

The operator "trace" is given by [22]

$$\text{trace}(A) = \sum_{i=1}^{n} a_{ii}.$$

3.2.2 Problem Formulation

Consider a plate which is under a known disturbance signal, i.e., the spatial domain $d(\xi, \zeta)$ of the acting signal on the plate is given. The objective of the control design is to achieve the desired performance specifications considering the spatial disturbance distribution.

3.2.3 Proposed Algorithm

One way to describe the performance specifications of a control system is in terms of minimizing the effects of disturbance $w(t)$ on the measured output $y(t)$.

To this end our optimal actuator placement policy employs $\mathcal{H}^2$ norm optimization rather than LQR method. When the distribution of disturbances is known our numerical investigation shows that the resulting optimal location differs from the one computed from controllability/LQR approaches. For example, if a gaussian disturbance distribution concentrates at the corner of the plate $(0.75a, 0.25b)$, the best actuator location offered by LQR and $\mathcal{H}^2$ control norm are different. The LQR suggests the best actuator location, based on the initial condition and the $\mathcal{H}^2$ control offers the best actuator location, with considering the disturbance distribution. For the all-clamped plate having the second modal shape as initial condition the best resulting placement from LQR method can be located at one of the four peaks of Figure 3.1. For the same condition, the best resulting actuator placement from $\mathcal{H}^2$ method is about the corner of the plate where the disturbance is applied as it is shown in Figure 3.2.

This result also can be predicted by reviewing the fundamentals of LQR and $\mathcal{H}^2$ optimization. The idea is to minimize $\|T_{yw}\|_2^2$

$$\|T_{yw}\|_2^2 = \text{trace}\Big[B_e^T L_c(\xi_p, \zeta_p) B_e\Big].$$

It should be remarked that $L_c(\xi, \zeta)$ for the current work is solved as the result of the following *Riccati equation* and not (3.10),

$$A^T L_c(\xi_p, \zeta_p) + L_c(\xi_p, \zeta_p) A - L_c(\xi_p, \zeta_p) B_c(\xi_p, \zeta_p) R^{-1} B_c^T(\xi_p, \zeta_p) L_c(\xi_p, \zeta_p) + Q = 0, \tag{3.11}$$

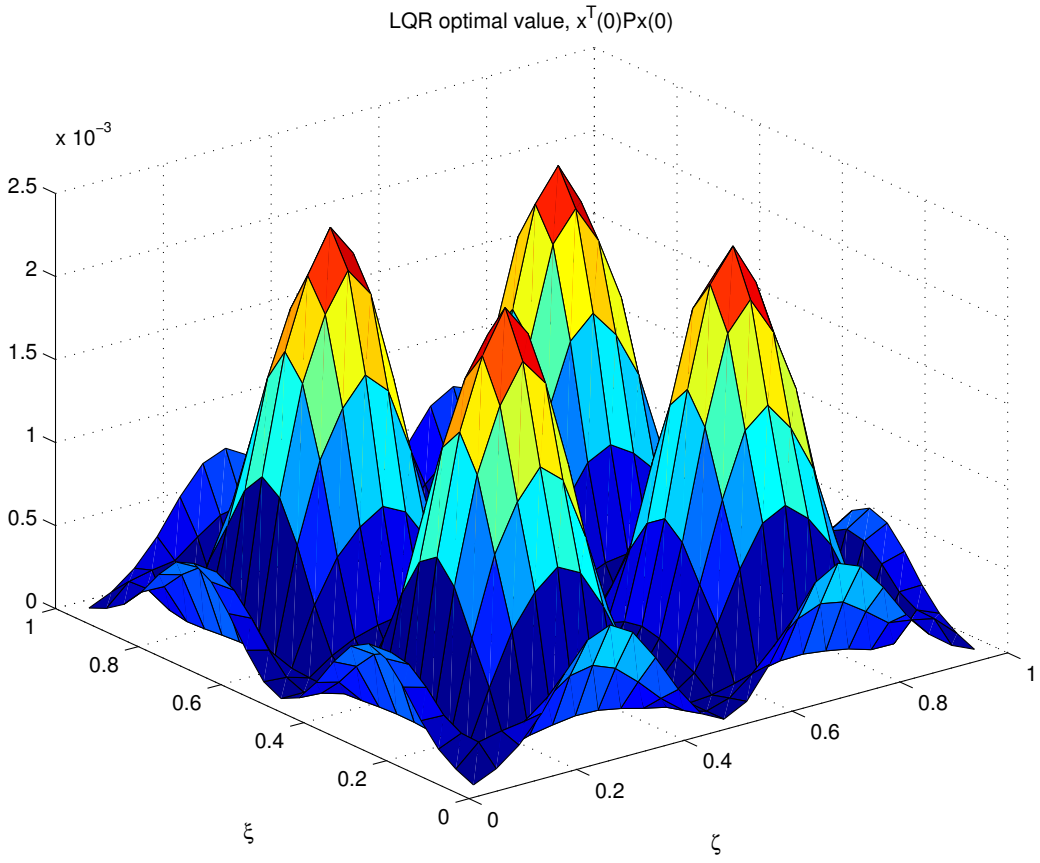

Figure 3.1: $LQR, \text{trace}(x(0)^T L_c x(0))$ placement for having disturbance distribution at the corner of the plate.

where Q and R are symmetric and $Q \geq 0$, $R > 0$.

The corresponding optimal gain k is solved as the result of an LQR problem. In the next section the process to obtain the feedback gain for the candidate locations is provided. The reason is stated in [20] as "*Optimization of the resulting closed loop transfer function* $\|T_{yw}\|_2^2$ *with respect to the admissible actuator locations would certainly produce a location that provides robustness with respect to spatial distribution but would not necessarily produce an optimal gain.*" This means that the actuator is placed at the best location based on the robust norm optimization, while L_c and feedback gain k are optimized by LQR techniques.

By substituting the value of L_c into $\|T_{yw}\|_2^2$ term, the actuator location which

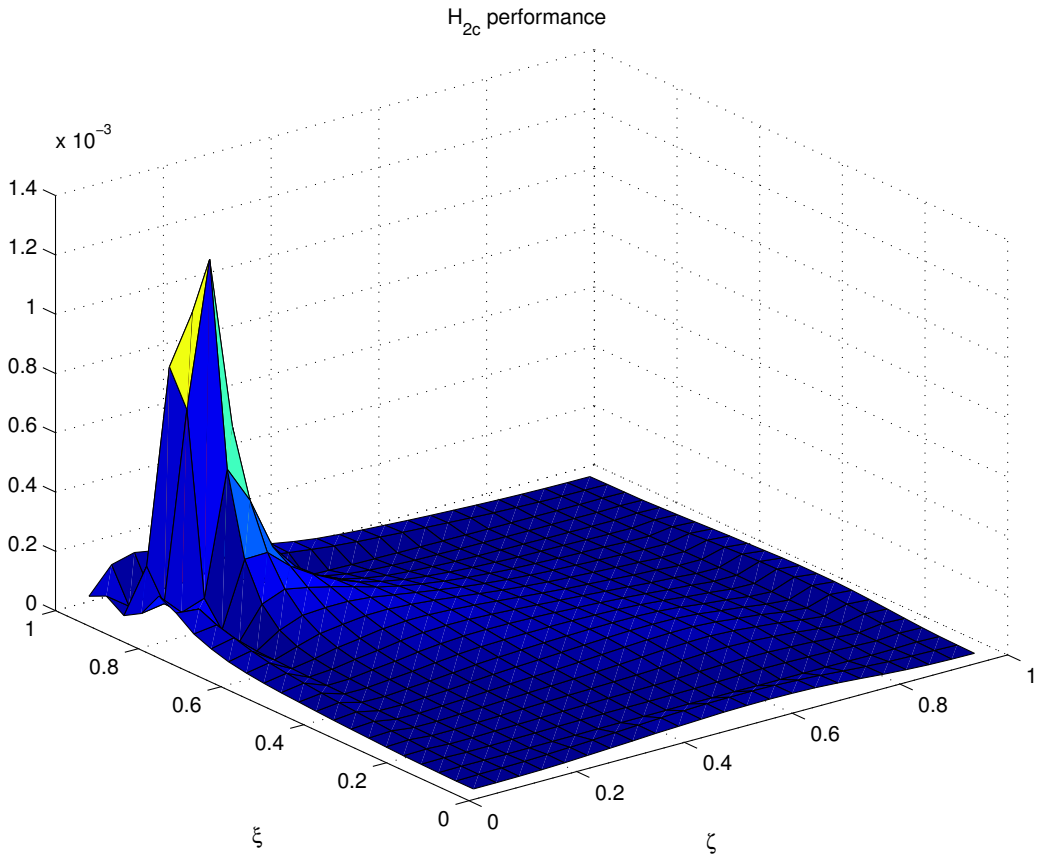

Figure 3.2: $\mathcal{H}^2$ placement for having disturbance distribution at the corner of the plate.

minimizes the $\mathcal{H}^2$ norm of the system, $\|T_{yw}\|_2^2$ is selected as the optimal location within N possible actuator candidates

$$(\xi_{opt}, \zeta_{opt}) = \arg \min_{(\xi,\zeta)\in\Theta_p} \text{trace}\Big[B_e^T L_c(\xi_p, \zeta_p) B_e\Big]. \tag{3.12}$$

3.2.4 Numerical Results for Different Disturbance Patterns

The objective is to find the best actuator location which provides optimal controllability with respect to various spatial distributions of disturbances. Based upon earlier results, [20], considering the disturbance patterns results in an optimal actuator placement and apparently provides a better performance. Figure 3.3 depicts

four different spatial disturbance profiles $d(\xi, \zeta)$ applied to the plate those are normalized such that their volume is unity:

1. Uniform disturbance distribution $D_a(\xi, \zeta) = \dfrac{1}{ab}$. The uniform disturbance distribution is smoothed to satisfy boundary conditions by four 3rd order polynomials, $Z_i(\xi) = a_{i3}\xi^3 + a_{i2}\xi^2 + a_{i1}\xi + a_{i0} = 0$, satisfying its boundary conditions as

$$
\begin{aligned}
&Z_1(0) = 0, Z_1(0.2a) = 1, Z_1'(0) = 0, Z_1'(0.2a) = 0,\\
&Z_2(a) = 0, Z_2(0.8a) = 1, Z_1'(a) = 0, Z_2'(0.8a) = 0,\\
&Z_3(0) = 0, Z_3(0.2b) = 1, Z_3'(0) = 0, Z_3'(0.2b) = 0,\\
&Z_4(b) = 0, Z_4(0.8b) = 1, Z_4'(b) = 0, Z_4'(0.8b) = 0.
\end{aligned}
$$

2. Gaussian disturbance distribution $D_b(\xi, \zeta) = G(0.5a, 0.5b, a/8, b/8)$ where

$$
G(\mu_\xi, \mu_\zeta, \sigma_\xi, \sigma_\zeta) = \frac{\exp\Big[-\frac{1}{2}\Big(\Big(\frac{\xi-\mu_\xi}{\sigma_\xi}\Big)^2 + \Big(\frac{\zeta-\mu_\zeta}{\sigma_\zeta}\Big)^2\Big)\Big]}{2\pi\sigma_\xi\sigma_\zeta}.
$$

3. Corner Gaussian disturbance profile $D_c(\xi, \zeta) = G(0.85a, 0.15b, a/56, b/56)$.

4. Second modal shape distribution $(m, n = 2)$ $D_d(\xi, \zeta) = \dfrac{\varphi_2(\xi)\psi_2(\zeta)}{\int_0^a |\varphi_2(\xi)|\, d\xi \int_0^b |\psi_2(\zeta)|\, d\zeta}$

where $\varphi_2(\xi), \psi_2(\zeta)$ are the second eigenfunctions [13], resulting in the $(2, 2)$ mode

$$
\begin{aligned}
\varphi_2(\xi) &= \Big[\cosh(\epsilon_2\xi/a) - \cos(\epsilon_2\xi/a) - \alpha_2\Big(\sinh(\epsilon_2\xi/a) - \sin(\epsilon_2\xi/a)\Big)\Big]\\
\psi_2(\zeta) &= \Big[\cosh(\epsilon_2\zeta/b) - \cos(\epsilon_2\zeta/b) - \alpha_2\Big(\sinh(\epsilon_2\zeta/b) - \sin(\epsilon_2\zeta/b)\Big)\Big],
\end{aligned}
$$

and where the constants ϵ_2 and α_2 are given in Table 3.1.

The related distribution of performance index, $\text{trace}\Big[B_e^T L_c(\xi_p, \zeta_p) B_e\Big]$, is shown in Figure 3.4 for each disturbance profile, where the disturbance distribution distribution, $d(\xi, \zeta)$, is considered as (D_a), (D_b), (D_c), and (D_d). For example, when

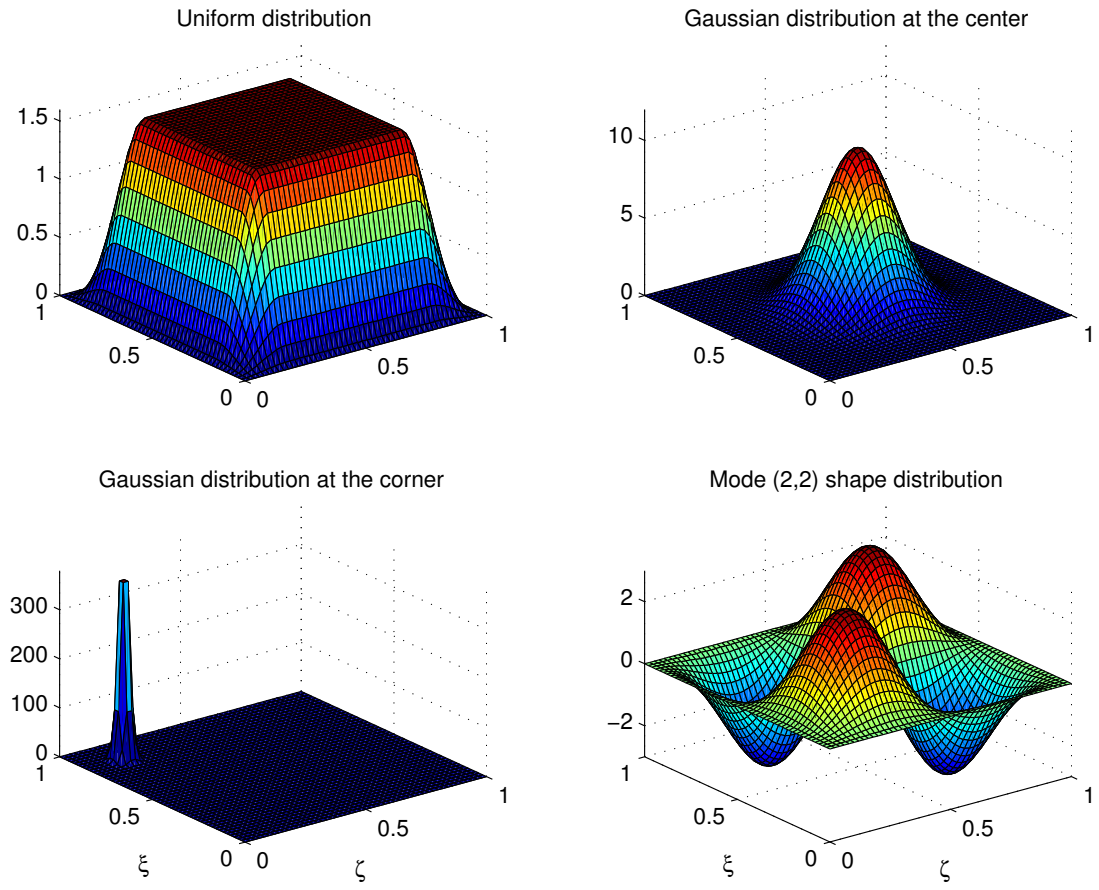

Figure 3.3: Different spatial disturbance profiles.

the spatial disturbance distribution concentrates at the corner of the plate (D_c), our numerical result verifies that the admissible actuator location closer to the peak of disturbance distribution minimizes the performance index rather than when the actuator is located at the center of the plate. As the disturbance pattern changes to a uniform disturbance distribution all over the plate (D_a), the corner actuator candidate does not result in cost function minimality anymore. Instead, as our former studies verify, the actuator located closer to the center of the plate is the best candidate which results in control optimality.

1. It should be noted that for a better visualization the $\mathcal{H}^2$ performance plotted is not directly $\|T_{yw}\|_2^2$ but it is $\Big(- \|T_{yw}\|_2^2 / \max(\|T_{yw}\|_2^2)\Big)$ in the Figure 3.4.

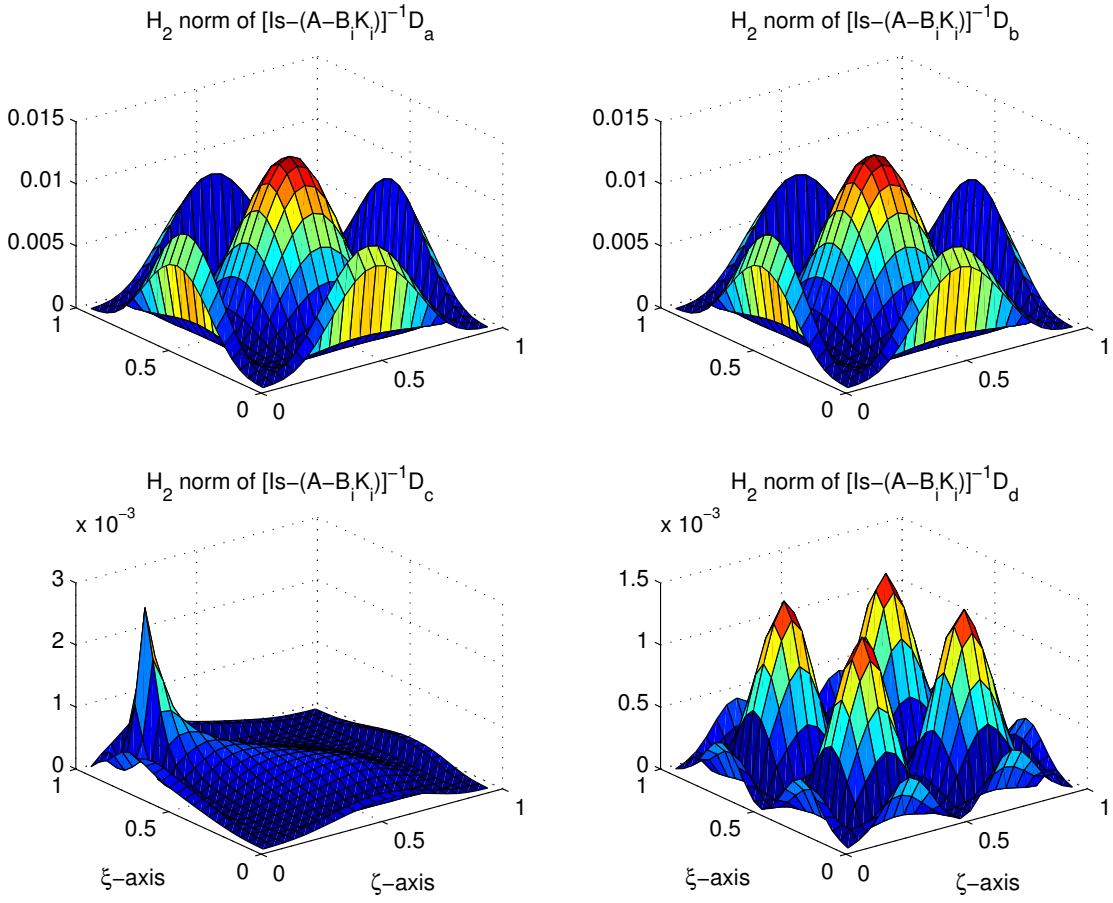

Figure 3.4: Distribution of $\mathcal{H}^2$ cost for each disturbance profile.

2. A number of 23×23 possible actuator locations are considered to be distanced uniformly on the plate in both ξ and ζ directions for a better visualization of Figure 3.3 and 3.4.

3. The number of modal/spline indices in ξ and ζ directions are respectively selected 15 and 14 ($m_\xi = 15, n_\zeta = 14$).

4. Matrices Q and R are selected

$$Q = \begin{pmatrix} K & 0_{m_\xi n_\zeta} \\ 0_{m_\xi n_\zeta} & 100M \end{pmatrix}, R = 10^{-6}.$$

5. The values of damping parameters for this part are assumed $\alpha_{d1} = 10^{-5}$ and $\alpha_{d2} = 10^{-3}$.

To visualize the performance of the applied control design, the energy norm of system including *kinetic* and *potential* energy, [25], is evaluated by

$$E(t) = \sqrt{\dot{\eta}^T(t) M \dot{\eta}(t) + \eta^T(t) K \eta(t)}. \tag{3.13}$$

The performance of the state feedback control system (3.3) is simulated for the case that plate is under (D_d) disturbance distribution. The result is shown in Figure 3.5 for both optimal actuator placement at $(0.29a, 0.29b)$, and non-optimal actuator placement at $(0.5a, 0.5b)$. The scheme that locates actuator with respect to the spatial disturbance pattern, exhibits an enhanced performance over the case of not considering the disturbance distribution.

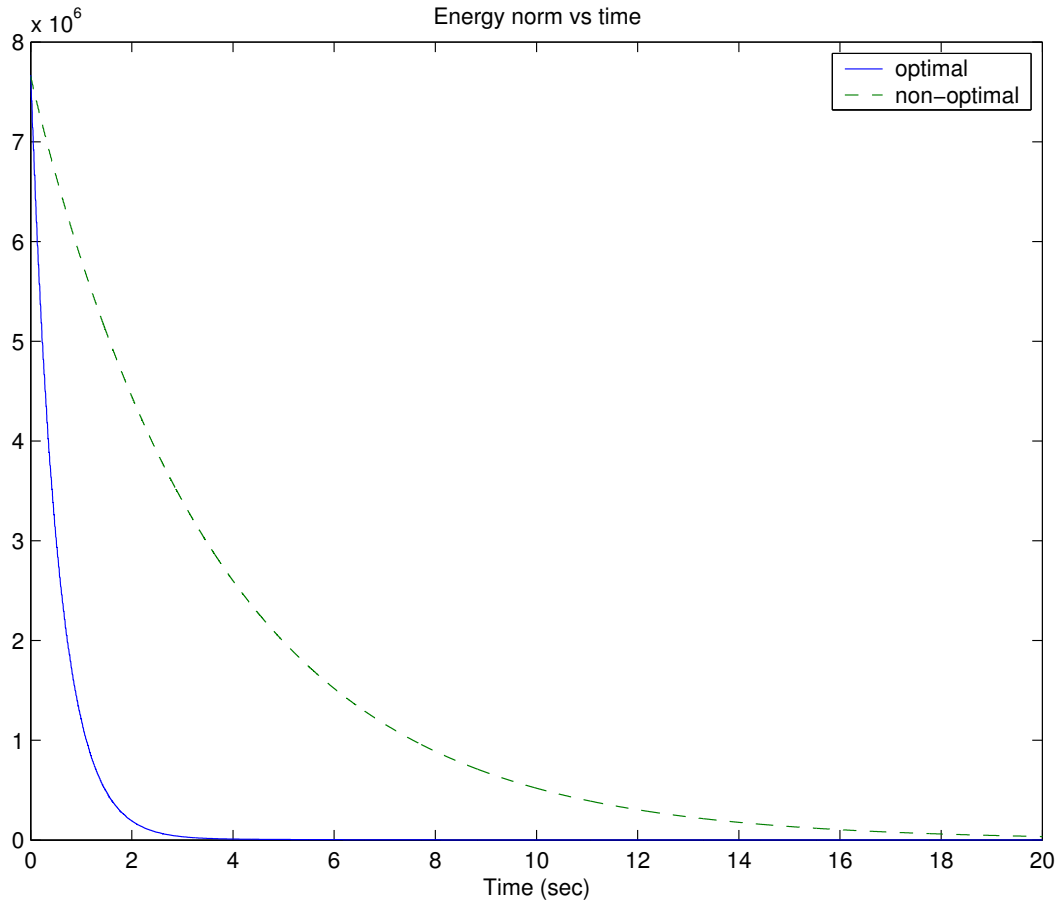

Figure 3.5: Energy norm of the system for non-moving disturbance distribution case.

3.3 Switching Control Algorithm

3.3.1 Linear-Quadratic Regulator/LQR

The *Linear-Quadratic Regulator* performance for a system such as (3.1) is defined by [26]

$$J = \int_0^\infty [x(t)^T Q x(t) + u(t)^T R u(t)] dt,$$

where Q and R are positive semidefinite and positive definite respectively. The problem here is assumed to be a regulation problem where the goal is to drive the state from the initial value to zero. To design a control system which minimizes

$\int_0^\infty x(t)^T Q x(t) dt$ leads to a design with larger input $u(t)$, [26]. A larger input causes the state of the system driving faster to zero than a smaller input. On the other hand, larger input values increases the amount of the input term $\int_0^\infty u(t)^T R u(t) dt$. A design that minimizes J represents a good balance between achieving a desired regulation and a reasonably sized input. It should be remarked that minimizing J causes the optimal solution which is mathematically tractable. In other words if it does not cause an optimal solution, minimizing J would be meaningless. System shown in (3.3) represents a feedback control system. The representative optimal performance J^* for any initial state condition in that case can be given by [26]

$$J^* = \int_0^\infty x(t)^T (Qx(t) + k^T R k) x(t) dt = x(0)^T P x(0),$$

where P is the solution to the *Riccati equation*

$$A^T P + PA - P B_c R^{-1} B_c^T P + Q = 0,$$

and, k must satisfy the necessary condition as it is proven in [26]

$$k = R^{-1} B_c P.$$

3.3.2 Problem Formulation

In the last section, the procedure to apply an optimal feedback control to a vibrating plate under a determined disturbance distribution is addressed. In this section the optimal control design is enhanced for a more general case. Consider the case that the disturbance signal is moving all over the plate which can be the case in real life situations. There are N piezoelectric patches which are implemented at controllable

locations of the plate. During each time sub-interval, $\Delta t = [t_i, t_{i+1}]$, the PZT actuator which results in control optimality is activated, and the switching policy keeps going until the vibration is damped to a certain level.

3.3.3 Proposed Algorithm

The method for optimal actuator placement employs the *Optimal LQ Regulator*. During each time sub-interval, $[t_i, t_{i+1}]$, the actuator resulting in the smallest cost-to-go performance index $J_i(\xi_p, \zeta_p)$ is activated. The index i represents the i_{th} sub-domain, $[t_i, t_{i+1}]$.

By applying the closed-loop feedback system, the performance measure for each PZT candidate location (ξ_p, ζ_p) at t_i can be defined by

$$J_i^*(\xi_p, \zeta_p) = \int_{t_i}^{\infty} x^T(t)(Q + k^T R k)x(t)dt = x^T(t_i)P(\xi_p, \zeta_p)x(t_i), \tag{3.14}$$

where P is the positive definite solution of the *Riccati equation*

$$A^T P(\xi_p, \zeta_p) + P(\xi_p, \zeta_p)A - P(\xi_p, \zeta_p)B_c(\xi_p, \zeta_p)R^{-1}B_c^T(\xi_p, \zeta_p)P(\xi_p, \zeta_p) + Q = 0.$$

N *Riccati equations* have been solved in order to find P for all N candidate PZT locations. By substituting the value of P into (3.14), the corresponding performance index can be achieved. Finally, the optimal placement within N possible actuator locations is obtainable during each Δt by

$$(\xi_{opt}, \zeta_{opt})_i = \arg \min_{(\xi_p, \zeta_p) \in \Theta_p} J_i^*(\xi_p, \zeta_p)\,,\ t \in [t_i, t_{i+1}) \tag{3.15}$$

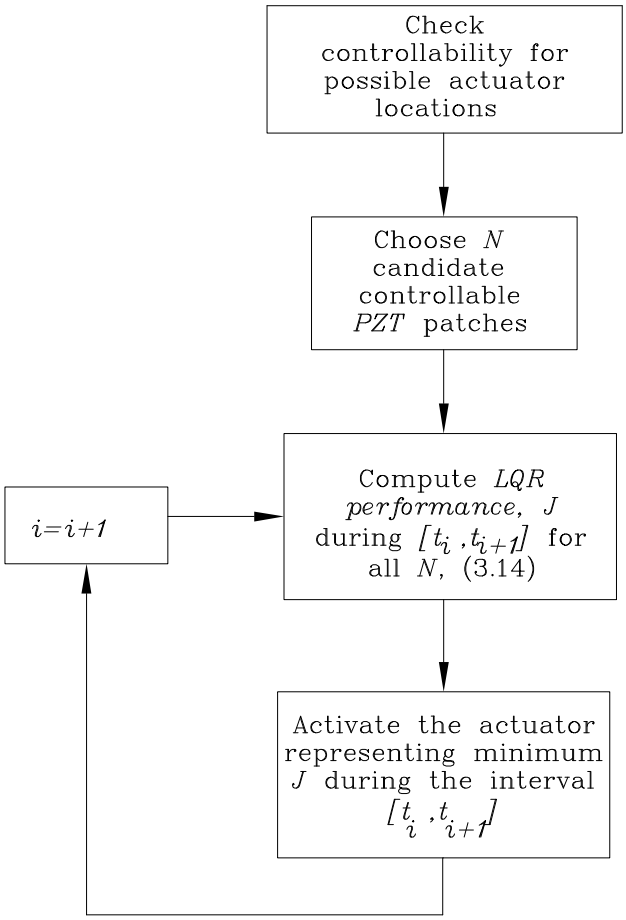

Figure 3.6: Switching PZT patches procedure chart.

while for LQR optimization the feedback gain, k, must satisfy

$$k(\xi_p, \zeta_p) = R^{-1} B_c(\xi_p, \zeta_p) P(\xi_p, \zeta_p).$$

For brevity the procedure is shown in Figure 3.6.

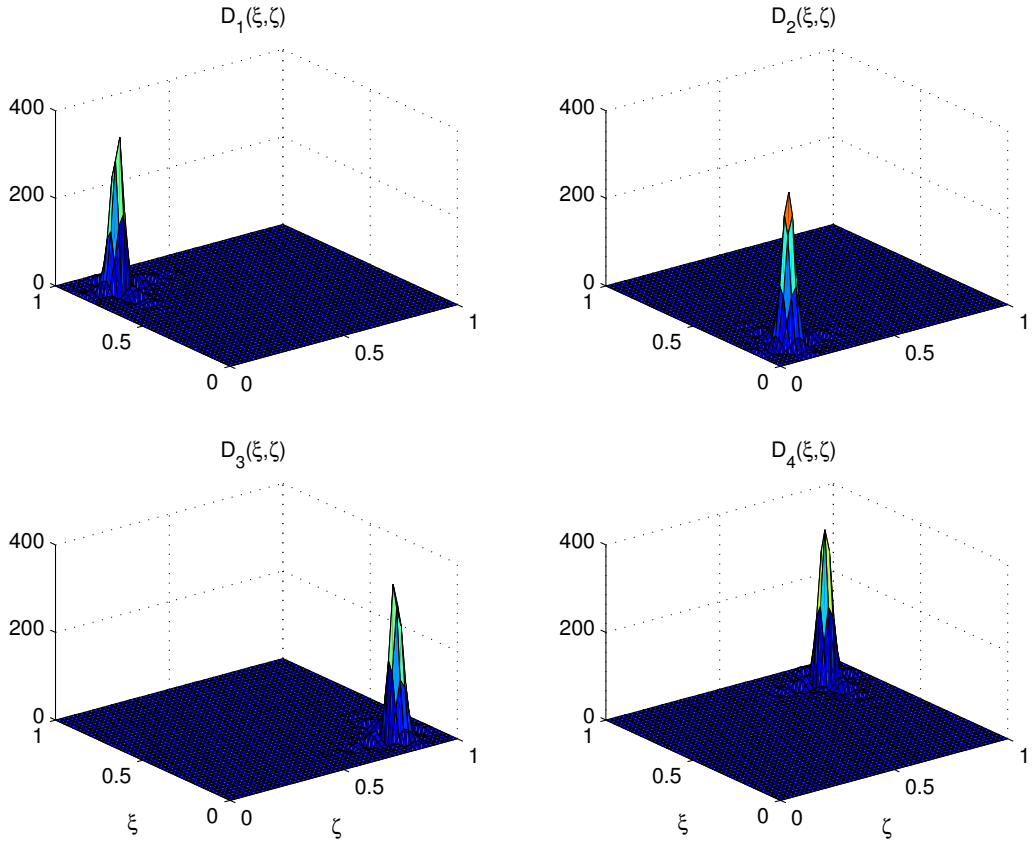

Figure 3.7: Different disturbance distribution for modelling a moving disturbance distribution.

3.3.4 Numerical Example for Switching Controller Methodology

A Gaussian disturbance profile moves counterclockwise from corner I to corner IV, as it is shown in Figure 3.9. At a given time the disturbance distribution can be D_1, D_2, D_3, or D_4 as shown in Figure 3.7. The procedure of the applied disturbance distribution and the temporal part, $w(t)$, is shown in Table (3.2).

Following Figure 3.6 the steps are as follows:

1. First, the uncontrollable locations based on controllability test are eliminated and a set of controllable actuator locations are considered as PZT candidate

Table 3.2: Excitation sequence of disturbance PZT patches.

Interval	Signal	$B_e(\xi, \zeta)$
$0 < t < 10$	$\sin(f_1 t) + \sin(f_2 t)$	D_1
$10 \leq t \leq 12$	–	–
$12 < t \leq 13$	$\sin(f_3 t)$	D_2
$13 < t \leq 15$	-	–
$15 < t \leq 16$	$\sin(f_4 t)$	D_3
$16 < t \leq 20$	–	–
$20 < t < 21$	$\sin(f_5 t)$	D_4
$21 \leq t < 25$	–	–
$25 \leq t < 26.5$	$\sin(f_6 t)$	D_1
$26.5 \leq t \leq 50$	–	–

locations as shown in Figure 3.8.

2. Based on the optimal control algorithm during each time step, the best actuator location is selected which results in the best performance of the system.

3. The switching actuator continues until the vibration of the system be damped to a desirable level, i.e, the energy norm of the system decreases to a certain level.

4. It should be remarked that for this numerical study, twenty five actuators are distributed uniformly on the plate as it is shown in Figure 3.8, while the number of spline indices in ξ and ζ directions are selected both 5 ($m_\xi = 5, n_\zeta = 5$). After checking the controllability condition (3.6), only ten possible locations are selected as controllable actuator placements.

5. The values of damping parameters in this part are assumed $\alpha_{d1} = 0.046$ and $\alpha_{d2} = 0$.

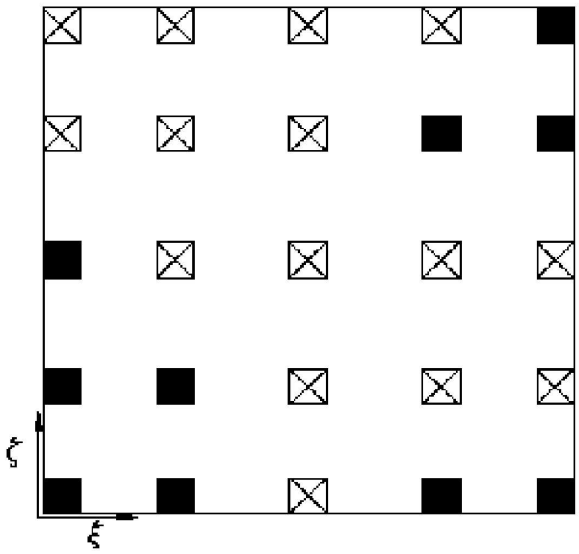

Figure 3.8: Twenty five candidate PZT locations in which ten of them are selected as controllable candidate placements.

As the disturbance signal moves around, the activated actuator switches to the best actuator during each time interval. To compare the performance of the applied switching controller system with the non-switching one, the energy norm of the system (3.10) is computed for open-loop, switching feedback control and a single-patch feedback controller placed at about (0.8a,0.8b). The numerical results, Figure 3.10, confirm that the switching control algorithm offers a better performance over the single-patch control design.

3.4 Velocity Sensor Observer

All the control methodologies have been discussed until now are all based on the assumption that the full state vector is available for measurement. Usually, it is not practical to measure the full state vector, but only a part of it.

It is also important to place the sensor(s) at an observable location(s). The

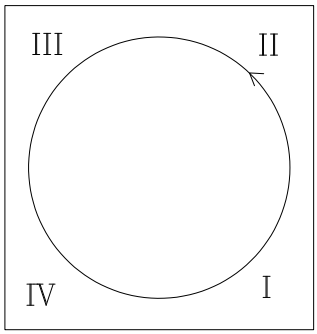

Figure 3.9: Spatial disturbance signal moving procedure.

observer system, designed for the present problem (3.1), has the form

$$\begin{aligned} \dot{\hat{x}}(t) &= A\hat{x}(t) + B_c(\xi_p, \zeta_p)u(t) + G(y(t) - C\hat{x}(t)) \\ y(t) &= Cx(t), \end{aligned} \tag{3.16}$$

where $\hat{x}(t)$ is a full dimensional observer state vector and G is a $2(m_\xi \times n_\zeta) \times r$ matrix and is called the observer gain matrix, where r indicates the number of sensors. It is assumed that the disturbance signal is unknown. In other words, the terms of disturbance distribution B_e and the temporal signal are not included in (3.16).

Using the *Kalman-Bucy filter*, the optimal observer gain matrix is given by

$$G = PC^T R_o^{-1},$$

where P_o is the solution to the following *Riccati equation*

$$AP_o + P_o A^T + V - PC^T R_o^{-1} C P_o = 0,$$

where R_o and V are noise intensities and are chosen in the way that the eigenvalues of $(A - GC)$ converge faster than the eigenvalues of the feedback control system

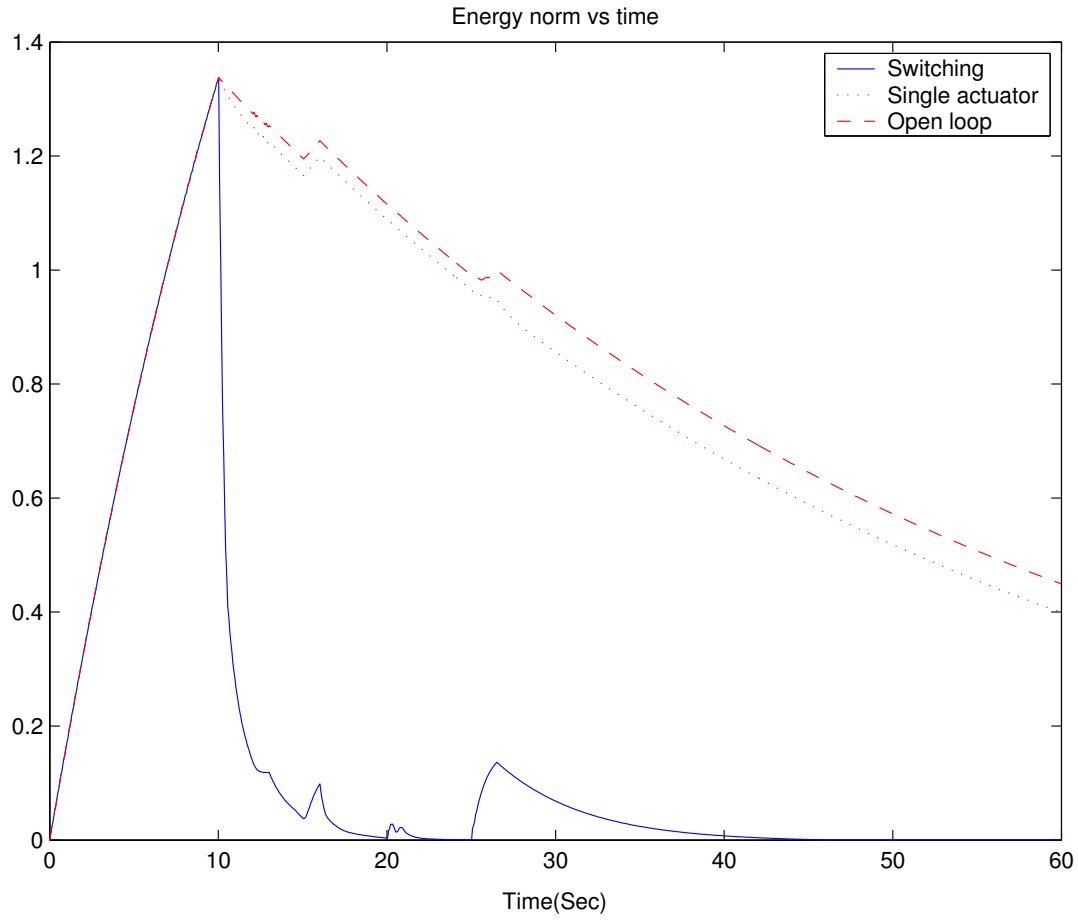

Figure 3.10: Energy norm of the system for moving disturbance distribution case.

$\Big(A - B_c(\xi_p, \zeta_p)k(\xi_p, \zeta_p)\Big)$ for all the candidate locations (ξ_p, ζ_p). As the observer poles lie in the deeper left half of the complex plane, it results in the faster convergence of $\hat{x}(t)$ to $x(t)$.

The optimal switching actuator placement is found by

$$(\xi_{opt}, \zeta_{opt})_i = \arg \min_{(\xi_p, \zeta_p) \in \Theta_p} J_i^*(\xi_p, \zeta_p),$$

where

$$J_i^*(\xi_p, \zeta_p) = \hat{x}^T(t_i) P(\xi_p, \zeta_p) \hat{x}(t_i)$$

where $P(\xi_p, \zeta_p)$ is the solution to the *Riccati Equation* and the gain representing the optimal location (ξ_p, ζ_p) is taken into account for the feedback control system

$$\dot{x}(t) = Ax(t) + B_c(\xi_p, \zeta_p)u(t) + B_e(\xi_p, \zeta_p)w(t)$$

where

$$u(t) = -k(\xi_p, \zeta_p)\hat{x}(t)$$

Introducing (3.16) and subtracting from (3.1), we obtain

$$\dot{x}(t) - \dot{\hat{x}}(t) = (A - GC)(x(t) - \hat{x}(t)) + B_e(\xi, \zeta)w(t). \tag{3.17}$$

By introducing $e(t)$

$$e(t) = x(t) - \hat{x}(t),$$

so that (3.17) can be rewritten in the form

$$\dot{e}(t) = (A - GC)e(t) + B_e(\xi, \zeta)w(t). \tag{3.18}$$

To search for the suitable locations for the sensor placement, those which result in observability for the fundamental modes are selected as candidates.

Consider the case of having ℓ velocity sensors placed at observable locations (ξ_o, ζ_o). The sensors measure velocity at the related points

$$y = \begin{pmatrix} \dot{W}(\xi_{o1}, \zeta_{o1}) \\ \vdots \\ \dot{W}(\xi_{o\ell}, \zeta_{o\ell}) \end{pmatrix} \tag{3.19}$$

where ℓ is the number of sensors.

For the observer simulation both the full state (3.1) and the observer system (3.16) are solved together.

By expanding (3.19), it can be written in the matrix form of

$$y = \begin{pmatrix} 0 & \dots & 0 & \varphi_1(\xi_{o1})\psi_1(\zeta_{o1}) & \dots & \varphi_{m_\xi}(\xi_{o1})\psi_{n_\zeta}(\zeta_{o1}) \\ \vdots & \vdots & \vdots & \vdots & \vdots & \vdots \\ 0 & \dots & 0 & \varphi_1(\xi_{ol})\psi_1(\zeta_{ol}) & \dots & \varphi_{m_\xi}(\xi_{oL})\psi_{n_\zeta}(\zeta_{oL}) \end{pmatrix} \begin{pmatrix} \eta_{11} \\ \vdots \\ \eta_{m_\xi n_\zeta} \\ \dot{\eta}_{11} \\ \vdots \\ \dot{\eta}_{m_\xi n_\zeta} \end{pmatrix}$$

or

$$y = Cx.$$

For the case of a single velocity sensor placed at the location (0.493a,0.493b), the energy norm of the simulated full state and the partial state are shown in Figure 3.11. It should be noted that zero initial condition is assumed for both cases. The numerical results verify that when the disturbance distribution signal is not known, the switching algorithm with output feedback offers an enhanced performance than the single patch with full state feedback and open loop cases.

The expressed algorithms are developed by the software $MATLAB$. The dimensions, and the material properties of the plate and PZT actuator can be given as the input of the program by user. The user can also select the number of possible actuators. For the simulation result, the values of parameters shown in Table 3.3 are selected.

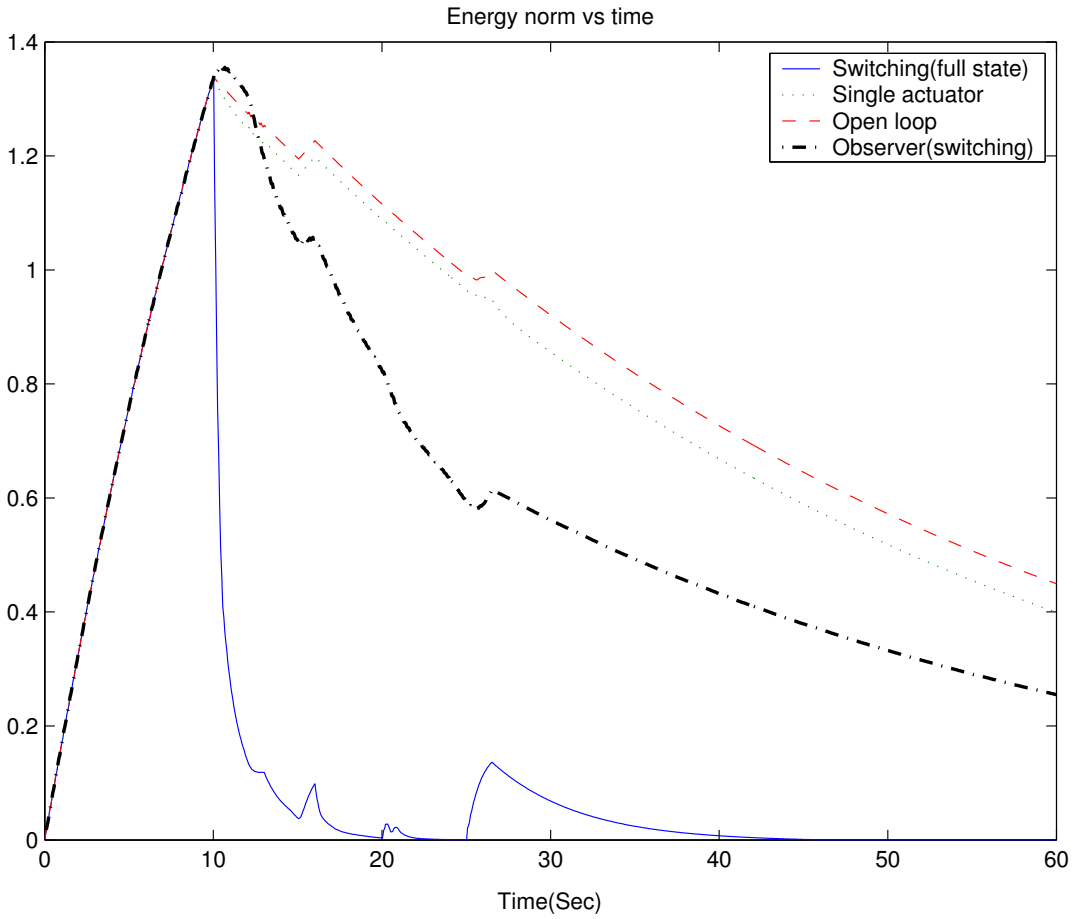

Figure 3.11: Energy norm of the system for the full state and observer-based feedback state in the switching actuator case.

Table 3.3: Properties of plate and a PZT patch.

Material	Aluminum
Dimensions of the plate $a \times b$	$1m \times 1m$
Thickness h	$0.002m$
Young's Modulus E	$69 \times 10^9 \frac{N}{m^2}$
Poisson's ratio ν	0.25
Flexural rigidity D_E	$49.067Nm$
PZT $L_{p\xi}(w_p)$	$0.07m$
PZT $L_{p\zeta}(w_p)$	$0.07m$
PZT Thickness h_p	$0.0002m$
PZT Young's Modulus E_p	$55 \times 10^9 \frac{N}{m^2}$
PZT Charge constant d_{31}	$-3.2 \times 10^{-10} \frac{m}{v}$
PZT Charge constant d_{32}	$-3.2 \times 10^{-10} \frac{m}{v}$

Chapter 4

Conclusion

4.1 Conclusion

In this thesis two fundamental problems are examined and the solutions to them are proposed: (i) in the first part of this thesis, a robust actuator placement with respect to varying disturbance distributions is considered. This is for the case that the spatial distribution of disturbance signal on the plate is known. The numerical result verifies that an optimal actuator placement with respect to the distribution of the disturbances offers a better performance; (ii) for the case that the plate has an unknown disturbance distribution, or the case where the disturbance signal moves randomly over the entire plate, switching actuator algorithm to control the vibration of the flexible plate based on LQR performance is presented. The suggested scheme confirms that the switching control algorithm offers a better performance over the single patch (non-switching) control design.

4.2 Future Work

Verification of the numerical simulation and proposed switching algorithm by implementing the experiment for an all-clamped plate is an exciting research that one can follow in future. It is suggested to take into account the following remarks and investigate the solutions to them.

4.2.1 Spillover Effects

It is clear that there is control spillover into the higher modes, so that some performance degradation can be expected during running the code. In this research, while the controllability is guaranteed for the first few modes, running the code for the higher modes sometimes resulted in the numerical errors and spillover phenomena. To reduce the effects of them: (i) one can enhance the controllability of the system for the wider range of excitation modes. This can be possible if one has access to the modal shapes of the plate for the higher modes, which for all-clamped plate this is not available for high modes. (ii) The results of the extensive numerical simulations suggest to consider different number of modes in ξ and ζ direction. It helps the condition (3.4) be valid for the higher number of modes. (iii) After simulating the control system for both square and rectangular plate, results show that the spillover effect reduces in the rectangular case ($a \neq b$). These notes can guide one to the point that the asymmetries can help avoiding the spillover effects and numerical errors.

4.2.2 Damping Coefficient

It should be noted that during running the code, it was found that the damping coefficient plays an important role in the result of the control system. The values

those are given to the code for damping parameters are $\alpha_{d1} = 0.046$ and $\alpha_{d2} = 0$. For example, the state feedback control system is also investigated for two more cases when $\alpha_{d1} = 0$ and $\alpha_{d2} = 0.046$, and $\alpha_{d1} = 10^{-5}$ and $\alpha_{d2} = 10^{-3}$. For these values, the control system does not have a good performance and the results are similar to open-loop. It is suggested to investigate more in the exact values of the damping parameters of the distributed systems.

4.2.3 PZT effects

The effects of the PZT actuator on the local properties of the plate such as thickness can be considered in future for more realistic results.

Bibliography

[1] Y. H Lim,*Finite-element Simulation of closedloop Vibration Control of Smart Plate under Transient Loading*, Journal of Smart Materials and Structures, 2003.

[2] K. M Liew,C. M Wang, Y. Xiang, and S. Kitipornchai, *Vibration of Mindlin Plates*, Elsevier Science Ltd, 1998.

[3] H.S. Tzou, and G. L. Anderson (both Editors), *Intelligent Structural Systems*, Kluwer Academic Publishers, 1992.

[4] C.R. Fuller, S.J. Elliot, and P. A. Nelson, *Active Control of Vibration*, New York: Academic, 1996.

[5] D. Halim, and S.O.R. Moheimani, *An Optimization Approach to Optimal Placement of Collocated Piezoelectric Actuators and Sensors on a Thin Plate*,Mechatronics Vol(13), 2003.

[6] M. A. Demetriou, and J. Borggaard, *Optimization of an integrated actuator placement and robust control scheme for distributed parameter processes subject to worst case spatial disturbance distribution*, Proceedings of the 2003 American Control Conference, Denver, Colorado, June 4-6, 2003.

[7] M. A. Demetriou, *Integrated Actuator Placement and Supervisory Switching in Flexible Structures under Spatiotemporal Disturbance Variations*, Proceedings

of the 2003 AIAA Guidance, Navigation, and Control Conference and Exhibit, Austin TX, August 11-14, 2003.

[8] M. A. Demetriou, *Activation Policy of Smart Controllers for Flexible Structures with Multiple Actuator/Sensor Pairs*, Proceedings of the Fourteenth International Symposium on Mathematical Theory of Networks and Systems, Perpignan, France, June 19-23, 2000.

[9] M. A. Demetriou, *Optimal switching policy of smart actuators in flexible structures*, Proceedings of the SPIE's Annual International Symposium on Smart Structures and Materials and NDE for Health Monitoring and Diagnostics, pp. 220-231, vol. 4326, Newport Beach, California, 4-8 March 2001.

[10] J. K. Hwang, C.H. Choi, C. K. Song, and J. M. Lee, *Robust LQG Control of An All-clamped Thin Plate with Piezoelectric Actuators/Sensors*,IEEE/ASME Transactions on Mechatronics, Vol. 2, No. 3, 1997.

[11] M. A. Demetriou, and M. Murugavel, *Experimental Implementation of An Optimal Actuator Switching Policy Algorithm in Flexible Structures*, SPIE, 2003.

[12] L. Meirovitch, *Dynamics and Control of Structures*, John Wiley and Sons, 1990.

[13] A. Leissa, *Vibration of Plates*, Acoustical Society of America, 1993.

[14] L. Meirovitch, *Elements of Vibration Analysis*, McGraw-Hill Book Company, 1986.

[15] W. Gawronski, *Actuator and Sensor Placement for Structural Testing and Control*, Journal of Sound and Vibration, 1997.

[16] H. S. Tzou, and H. Q. Fu *A study of Segmentation of Distributed Piezoelectric Sensors and Actuators*, Journal of Sound and Vibration, 1994.

[17] A. Hac, and L. Liu *Sensor and Actuator Location in Motion Control of Flexible Structures*, Journal of Sound and Vibration, 1993.

[18] P. M. Prenter, *Spline and Variational Methods*, Wiley-Masson, New york, 1975.

[19] M. Murugavel, *M.S. Thesis: Implimentation of an Actuator Placement, Switching Algorithm for Active Vibration Control in Flexible Structure*, W.P.I., 2002.

[20] M. A. Demetriou, T. Moghani, *Robust Actuator Placement in Flexible Plates Subject to Worst-Case Spatial Distribution of Disturbances*, Proceedings of the American Control Confrence, Boston, June 30-July 2, 2004.

[21] K. Zhou, *Essentials of Robust Control*, Prentice-Hall, Inc., 1998.

[22] E. Kreyszig, *Advanced Engineering Mathematics*, John Wiley and Sons,Inc., 1993.

[23] A. Preumont, *Vibration Control of Active Structures: An Introduction*, Kluwer Academic Publishers, 1997.

[24] S.O.R. Moheimani, *An Experimental Verification of a Reduced Order Transfer Function of a Piezoelectric Laminate Beam*, Proceedings of the 38^{th} Conference on Decision Control, Phoenix, Arizona, 1999.

[25] R. E. Skelton, T. Iwasaki, and K. Grigoriadis, *A Unified Algebric Approach to Linear Control Design*, Taylor and Francis Inc., John Wiley and Sons, New York, 1988.

[26] P. R. Belanger, *Control Engineering; A Modern Approach*, Saunders College Publishing, 1995.

[27] *http://www31.brinkster.com/nckh/data/groups/mt/2.htm*